Relation between spin Hall effect and anomalous Hall effect in 3d ferromagnetic metals

Yasutomo Omori,[1] Edurne Sagasta,[2] Yasuhiro Niimi,[1,3,*] Martin Gradhand,[4] Luis E. Hueso,[2,5] Fèlix Casanova,[2,5] and YoshiChika Otani[1,6,†]

[1]*Institute for Solid State Physics, University of Tokyo, Kashiwa, Chiba 277-8581, Japan*
[2]*CIC nanoGUNE, 20018 Donostia-San Sebastian, Basque Country, Spain*
[3]*Department of Physics, Graduate School of Science, Osaka University, Toyonaka, Osaka 560-0043, Japan*
[4]*H. H. Wills Physics Laboratory, University of Bristol, Bristol BS8 1TL, United Kingdom*
[5]*IKERBASQUE, Basque Foundation for Science, 48011 Bilbao, Basque Country, Spain*
[6]*RIKEN-CEMS, 2-1 Hirosawa, Wako, Saitama 351-0198, Japan*

We study the mechanisms of the spin Hall effect (SHE) and anomalous Hall effect (AHE) in 3d ferromagnetic metals [Fe, Co, permalloy ($Ni_{81}Fe_{19}$; Py), and Ni] by varying their resistivities and temperature. At low temperatures where the phonon scattering is negligible, the skew scattering coefficients of the SHE and AHE in Py are related to its spin polarization. However, this simple relation breaks down for Py at higher temperatures as well as for the other ferromagnetic metals at any temperature. We find that, in general, the relation between the SHE and AHE is more complex, with the temperature dependence of the SHE being much stronger than that of AHE.

I. INTRODUCTION

The spin Hall effect (SHE) and its inverse (ISHE) enable us to interconvert spin and charge currents in the transverse direction and are widely recognized as essential methods to generate and detect spin currents in spintronic devices [1–3]. Since the original predictions of the SHE [4,5], it has been experimentally investigated in a variety of nonmagnetic materials with strong spin-orbit interactions such as III-V semiconductors [6,7], 4d and 5d transition metals [8–16], alloys [17–20], oxides [21], and organic materials [22]. The mechanism of the SHE can be extrinsic or intrinsic. The former depends on the combination of the host metal and impurities [23–25], while the latter depends on the detailed properties of the momentum-space Berry phase [26,27]. These mechanisms are the same as for the anomalous Hall effect (AHE) in ferromagnetic metals (FMs), which has been intensively studied for many years [28]. Thus, it has been commonly accepted that the SHE shares the same origin as the AHE [29].

It was experimentally verified that not only the ISHE [30–32] but also the SHE [33–37] occur in FMs with finite spin polarization. In FMs, both spin and charge accumulations can exist [38] and are detected as the SHE and the AHE, respectively [see Fig. 1(a)]. Very recently, the control of the spin accumulation by manipulating the magnetization of the ferromagnet has been achieved experimentally [33–36] after its theoretical prediction [38]. Das *et al.* [33] used the term "anomalous SHE" to describe this mechanism. The anomalous SHE can be understood by generalizing the spin conductivity σ_{ij}^s to $\sigma_{ij}^s(M)$ allowing for the anisotropy of σ_{ij}^s as discussed by Seemann *et al.* [39]. Here ij are the spatial directions, s refers to the direction of the spin and M is the global magnetization of the ferromagnet. For the simplest contribution to this general response, in other words, $M \propto s$, it was suggested that the SHE and AHE in FMs are related via the spin polarization [31]. However, it has not been experimentally verified if this simple relation is general, and therefore valid for all the FMs and all the mechanisms. From a theoretical viewpoint, such a relation might hold in the limit of diffusive transport [40] but is not expected to hold in general.

In this work, we present a detailed investigation of the relation between the SHE and the AHE in four different 3d FMs, i.e., Fe, Co, permalloy ($Ni_{81}Fe_{19}$; Py), and Ni. By changing the residual resistivity of the FM at low temperatures, the skew scattering contribution (one of the extrinsic mechanisms) [41] can be separated from other contributions. It turns out that the aforementioned relation between the SHE and AHE holds for the skew scattering term in Py. However, this simple relation is not valid for the other mechanisms in Py and for the other FMs. The SHE in the 3d FMs has much stronger temperature dependence than the AHE. We discuss a possible scenario to explain the observed results.

II. EXPERIMENTAL DETAILS

To perform the SHE measurements in the 3d FMs, we adopted the spin absorption method in the lateral spin valve structure [13,15,16,18–21]. This method enables us to estimate the spin diffusion length and the spin Hall angle (θ_{SHE}) on the same device. The SHE devices were fabricated on SiO_2/Si substrates with multiple-step electron beam lithography followed by metal deposition and liftoff. We first patterned two 100-nm-wide wires and deposited Py by 30 nm in thickness by electron beam evaporation. The two Py wires are separated by a length (L) of 1 μm, as illustrated in Fig. 1(b). One of the Py wires is used as a spin current injector, while

*niimi@phys.sci.osaka-u.ac.jp
†yotani@issp.u-tokyo.ac.jp
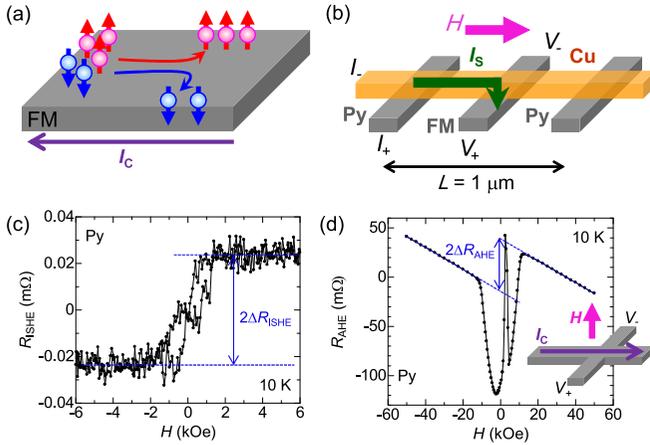
FIG. 1. (a) Intuitive schematic of the SHE and the AHE in FM. Spin and charge accumulations appear in the transverse direction with respect to the incident current I_C and are detected as the SHE and the AHE, respectively. (b) Schematic of a lateral spin valve for the spin absorption method to measure the ISHE in FM. The magnetic field H is applied along the Cu wire. (c) Inverse spin Hall resistance R_{ISHE} of the middle Py wire (20 nm in thickness) as a function of H at 10 K using the configuration shown in (b). The ISHE signal (ΔR_{ISHE}) is defined in the figure. (d) Anomalous Hall resistance R_{AHE} of Py as a function of H at 10 K. The AHE signal (ΔR_{AHE}) is defined in the figure. The inset shows a part of a Hall bar for the AHE measurement. The magnetic field H is applied perpendicular to the plane. Compared to the SHE configuration, the field direction is rotated by 90°.

the other is used to estimate the spin diffusion length of our target wire, as detailed in the Supplemental Material [42]. In the second step, the target 3d FM wire (hereafter middle wire) with the width (w_M) of 200 nm was placed just in the middle of the two Py wires and a 5- to 30-nm-thick 3d FM (Fe, Co, Py, or Ni) was deposited with electron beam evaporation. In the third step, a 100-nm-wide and 100-nm-thick Cu strip was bridged on top of the three wires with a Joule heating evaporator. Before the Cu evaporation, an Ar-ion milling treatment was performed to achieve transparent interfaces. For the AHE measurements, a 20-μm-long and 3-μm-wide Hall bar was patterned with electron beam lithography and the FM (5 to 30 nm in thickness) was deposited at the same time as the SHE devices were prepared. We then capped all the devices with Al_2O_3 using radio-frequency magnetron sputtering to protect them from oxidization. All the electric transport measurements were performed in a ^{4}He flow cryostat using the lock-in technique.

III. RESULTS AND DISCUSSIONS

A. SHE and AHE in Py

When an electric current I_C is injected from Py to the left side of Cu as shown in Fig. 1(b), spin accumulation is created at the interface and diffuses in the Cu bridge. In this process, a pure spin current I_S flows in the Cu channel on the right side. Most of I_S is then absorbed into the middle wire and converted into charge current via the ISHE, which is detected

as a voltage drop $V_{ISHE}(= V_+ - V_-)$. The ISHE resistance $R_{ISHE} = V_{ISHE}/I_C$ is measured by sweeping the external magnetic field H along the Cu channel. It is saturated when the magnetization of the Py wire is fully polarized. The difference of R_{ISHE} between the positive and negative saturated magnetic fields is the ISHE signal, defined as $2\Delta R_{ISHE}$. As shown in Fig. 1(c), a positive $\Delta R_{ISHE}(\sim25\ \mu\Omega)$ was obtained at 10 K for a 20-nm-thick Py middle wire with the longitudinal resistivity ρ_{xx} of 22 $\mu\Omega$ cm.

We also confirmed the reciprocity in the present system for FM. This can be realized by exchanging the electrodes ($V_+ \leftrightarrow I_+$, $V_- \leftrightarrow I_-$) on the same device and measuring the direct SHE, as detailed in the Supplemental Material [42]. It is well known that the AHE occurs in FMs as a result of the breaking of time-reversal symmetry. However, the Onsager reciprocal relation holds for the SHE in FMs [43] because the *total* number of spin-up and spin-down electrons is always kept constant.

By using the spin transport model proposed by Takahashi and Maekawa [44], the spin Hall resistivity $-\rho_{xy}^{SHE}$ can be estimated as follows:

$$-\rho_{xy}^{SHE} = \rho_{yx}^{SHE} = \theta_{SHE}\rho_{xx} = \frac{w_M}{x}\left(\frac{I_C}{\bar{I}_S}\right)\Delta R_{ISHE}, \quad (1)$$

where x is the shunting factor and $\bar{I}_S$ is the effective spin current absorbed into the FM middle wire. When $\bar{I}_S$ is converted into charge current in the middle wire, a part of the charge current is shunted by the Cu bridge on the middle FM wire. The shunting factor x has been calculated with a finite elements method using SPINFLOW 3D [16,19]. $\bar{I}_S$ can be determined from nonlocal spin valve measurements with and without the middle wire [42]. $\bar{I}_S$ is also related to the spin diffusion length of the middle FM wire.

We next measured the AHE with a Hall bar pattern, prepared at the same time as the SHE device. By applying an out-of-plane magnetic field and flowing I_C in the longitudinal direction of the Hall bar, a transverse voltage drop $V_{AHE}(= V_+ - V_-)$ is detected, as sketched in the inset of Fig. 1(d). Figure 1(d) shows a typical $R_{AHE} = V_{AHE}/I_C$ vs H curve for Py at 10 K. Although there are two backgrounds, namely, normal Hall resistance and planar Hall resistance in between ±10 kOe [45], a clear positive AHE signal ΔR_{AHE} can be extracted. From ΔR_{AHE}, we obtain the anomalous Hall resistivity defined as

$$-\rho_{xy}^{AHE} = \rho_{yx}^{AHE} = \theta_{AHE}\rho_{xx} = t\Delta R_{AHE}, \quad (2)$$

where θ_{AHE} is the anomalous Hall angle and t is the thickness of the Hall bar.

By plotting $-\rho_{xy}^{SHE}$ and $-\rho_{xy}^{AHE}$, obtained with Eqs. (1) and (2), as a function of ρ_{xx}, the detailed mechanisms can be addressed as shown in previous works [16,46,47]. For this purpose, the recent scaling equation proposed by Hou *et al.* [46] is useful:

$$-\rho_{xy}^H = \alpha_{ss}^H\rho_{xx,0} + \beta_0^H(\rho_{xx,0})^2 + \gamma^H\rho_{xx,0}\rho_{xx,T} + \beta_1^H(\rho_{xx,T})^2, \quad (3)$$

where H refers to the SHE or AHE, $\rho_{xx,0}$ is the residual resistivity at low temperature (in the present case, at 10 K),
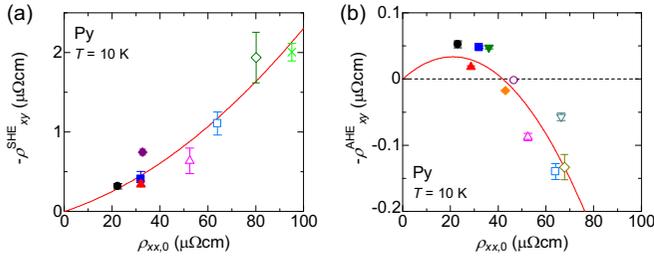
FIG. 2. (a) Spin Hall resistivity $-\rho_{xy}^{\mathrm{SHE}}$ and (b) anomalous Hall resistivity $-\rho_{xy}^{\mathrm{AHE}}$ in Py as a function of $\rho_{xx,0}$ at 10 K. The solid lines are the best fits with Eq. (2). The same symbol is used in (a) and (b) if the Py deposition is done at the same time for the SHE and AHE samples. The dotted line in (b) indicates $-\rho_{xy}^{\mathrm{AHE}} = 0$.

FIG. 3. (a) Spin Hall angle θ_{SHE} and (b) anomalous Hall angle θ_{AHE} measured at 10 K as a function of the number of electrons in the outermost shell. The thickness of the the 3d FMs is 20 nm. The dotted lines in (a) and (b) indicate $\theta_{\mathrm{H}} = 0$.

$\rho_{xx,T}(= \rho_{xx} - \rho_{xx,0})$ is the resistivity induced by phonons, and $\alpha_{\mathrm{ss}}^{\mathrm{H}}$ is the skew scattering angle due to impurities or grain boundaries. As detailed in Ref. [46], the side-jump terms due to static (impurities or grain boundaries) and dynamic (phonons) scattering sources as well as the intrinsic contribution originating from the band structure [48–54] are entangled in β_0^{H}, γ^{H}, and β_1^{H} in a complex manner. Nevertheless, as discussed in Ref. [46], the effect of the intrinsic Berry curvature is most strongly reflected in the β_1^{H} term.

First, to simplify Eq. (3), we focus on the low-temperature part where the phonon contribution is negligible and consider the case of Py. By substituting $\rho_{xx,T} = 0$ in Eq. (3), a simplified equation can be obtained:

$$-\rho_{xy}^{\mathrm{H}} = \alpha_{\mathrm{ss}}^{\mathrm{H}}\rho_{xx,0} + \beta_0^{\mathrm{H}}(\rho_{xx,0})^2. \qquad (4)$$

In order to determine $\alpha_{\mathrm{ss}}^{\mathrm{H}}$ and β_0^{H}, the SHE and AHE of Py have to be measured in a wide $\rho_{xx,0}$ range. For this purpose, we changed the thickness of the Py wire (from 5 to 30 nm) and also the deposition rate (from 0.04 nm/s to 0.08 nm/s), as already demonstrated in our previous work for Pt [16]. Figures 2(a) and 2(b) show $-\rho_{xy}^{\mathrm{SHE}}$ and $-\rho_{xy}^{\mathrm{AHE}}$ of Py at 10 K as a function of $\rho_{xx,0}$, respectively. $-\rho_{xy}^{\mathrm{SHE}}$ increases with increasing $\rho_{xx,0}$, while $-\rho_{xy}^{\mathrm{AHE}}$ decreases with $\rho_{xx,0}$. By fitting $-\rho_{xy}^{\mathrm{SHE}}$ and $-\rho_{xy}^{\mathrm{AHE}}$ with Eq. (4), the skew scattering term $\alpha_{\mathrm{ss}}^{\mathrm{H}}$ and the combination of the side-jump and intrinsic contributions β_0^{H} can be obtained as follows: $\alpha_{\mathrm{ss}}^{\mathrm{SHE}} = 1.0 \pm 0.4\%$, $\alpha_{\mathrm{ss}}^{\mathrm{AHE}} = 0.32 \pm 0.1\%$, $\beta_0^{\mathrm{SHE}} = 131 \pm 60\ \Omega^{-1}\,\mathrm{cm}^{-1}$, and $\beta_0^{\mathrm{AHE}} = -76 \pm 20\ \Omega^{-1}\,\mathrm{cm}^{-1}$. $\alpha_{\mathrm{ss}}^{\mathrm{AHE}}$ and β_0^{AHE} are in good agreement with previous reports [45,55].

Interestingly, the ratio of the AHE and SHE in Py for the skew scattering contribution $\alpha_{\mathrm{ss}}^{\mathrm{AHE}}/\alpha_{\mathrm{ss}}^{\mathrm{SHE}} = 0.32$ is a reasonable value for the spin polarization p of Py [18,56]. In other words, for the skew scattering, the relation between the AHE and SHE can be expressed as

$$\rho_{xy}^{\mathrm{AHE}} = p\rho_{xy}^{\mathrm{SHE}}. \qquad (5)$$

This can be understood intuitively as follows. In FMs, incident spin-up and -down electrons are deflected to the transverse opposite directions, as illustrated in Fig. 1(a). Since the number of spin-up electrons (3 in the sketch) is larger than that of spin-down electrons (2 in the sketch), there is a finite charge accumulation (the difference of the deflected electrons, i.e., 1 in the sketch) along the transverse direction with respect to the
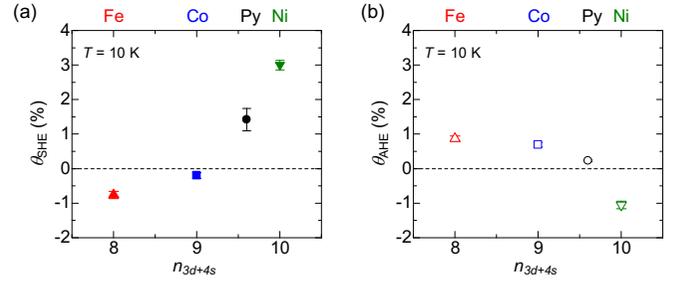
incident current direction, which can be detected as an anomalous Hall voltage. On the other hand, the spin accumulation is proportional to the difference of spin directions (5 in the sketch), which can be detected as a spin Hall voltage. Thus, the ratio of the AHE and SHE is indeed the spin polarization [$p = (3 - 2)/(3 + 2) = 0.2$ in the sketch of Fig. 1(a)].

In fact, this simple picture can be applied for diffusive scattering systems such as Py. As we detail in Ref. [42], Eq. (5) can be derived in Mott's two-current model [57] under the specific assumption $\frac{\rho_{xy}^{\uparrow}}{\rho_{xx}^{\uparrow}} = -\frac{\rho_{xy}^{\downarrow}}{\rho_{xx}^{\downarrow}}$. Here, $\rho_{ij}^{\uparrow}$ and $\rho_{ij}^{\downarrow}$ are the spin-up and -down resistivity tensor elements. Py is a random alloy composed of Ni and Fe. The anisotropy on the Fermi surface should be suppressed and lead to more isotropic scattering properties. Thus, the Hall angle is essentially a spin-independent property averaged over all the contributing states. This supports the finding that the simplified relation holds for the skew scattering in Py.

B. SHE and AHE in other 3d FMs

However, such a simple picture does not work for the other 3d FMs. The electronic states can be quite anisotropic because of the complicated band structure of 3d FMs. Those states should show distinct effective spin-orbit couplings for spin-up and -down electrons. Thus, the above specific assumption can break down. We show θ_{SHE} and θ_{AHE} at $T = 10$ K for the 3d FMs in Figs. 3(a) and 3(b), respectively. As in the case of the intrinsic SHEs in 4d and 5d transition metals [13,26,27],
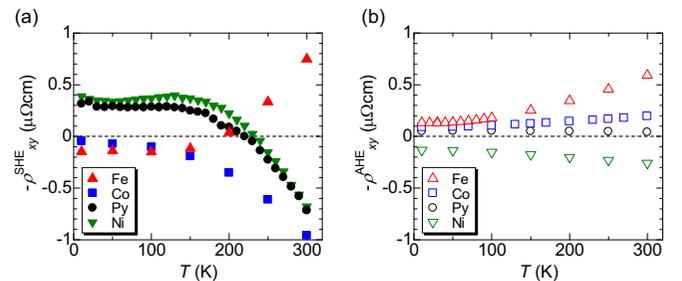
FIG. 4. The temperature dependence of (a) spin Hall resistivity $-\rho_{xy}^{\mathrm{SHE}}$ and (b) anomalous Hall resistivity $-\rho_{xy}^{\mathrm{AHE}}$ in four FMs (Py, Fe, Co, and Ni). The thickness of the four FMs is 20 nm both for the SHE and AHE measurements.
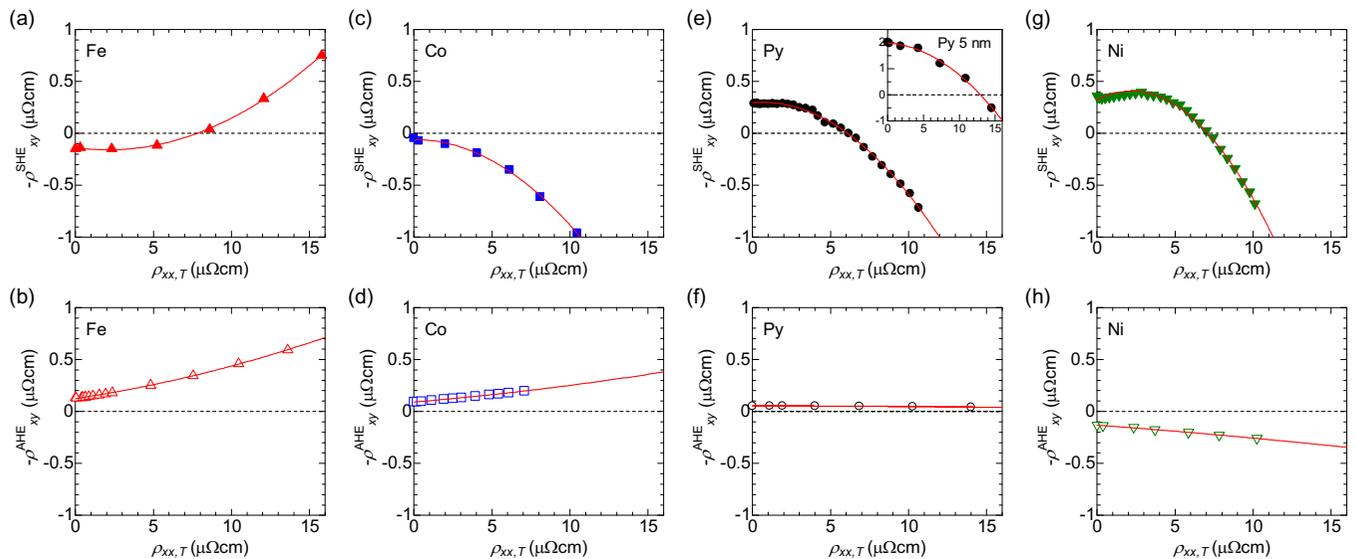
FIG. 5. Spin Hall resistivity $-\rho_{xy}^{\text{SHE}}$ and anomalous Hall resistivity $-\rho_{xy}^{\text{AHE}}$ in four FMs (Fe, Co, Py, and Ni) at finite temperatures. $-\rho_{xy}^{\text{SHE}}$ as a function of $\rho_{xx,T}$ in (a) Fe, (c) Co, (e) Py, and (g) Ni. Anomalous Hall resistivity $-\rho_{xy}^{\text{AHE}}$ as a function of $\rho_{xx,T}$ in (b) Fe, (d) Co, (f) Py, and (h) Ni. $\rho_{xx,T}$ varies by changing temperature from 10 to 300 K. The solid lines are the best fits of the data to Eq. (3). The thickness of the four FMs is 20 nm both for SHE and AHE measurements except for the inset in (e). The inset in (e) shows $-\rho_{xy}^{\text{SHE}}$ of 5-nm-thick Py wire. For the fitting with Eq. (3), the same parameter $\beta_1^{\text{SHE}} = -10.1(\times 10^3 \ \Omega^{-1} \text{cm}^{-1})$ was used both for 20-nm and 5-nm-thick Py wires.

θ_{SHE} is expected to change the sign from negative to positive with increasing the number of electrons in the outer shell [32]. Such a tendency can be seen clearly in θ_{SHE} of the 3*d* FMs in Fig. 3(a). However, the sign of θ_{SHE} is opposite to that of θ_{AHE} for Fe, Co, and Ni. Even in the case of Py, θ_{AHE} is negative when $\rho_{xx,0}$ is more than 40 $\mu\Omega$ cm, as shown in Fig. 2(b). This obviously shows that Eq. (5) is not general and the detailed band structure of the electron orbitals has to be taken into account, as mentioned above.

So far, we have focused on the low-temperature parts of the SHE and AHE. To address the effect of dynamic disorders, we next discuss the temperature dependencies of the SHE and AHE in Figs. 4(a) and 4(b), respectively. The temperature dependence of the SHE is much stronger than that of the AHE. For Fe, Py, and Ni, the sign of $-\rho_{xy}^{\text{SHE}}$ is changed at 200–250 K, while such a sign change cannot be seen for $-\rho_{xy}^{\text{AHE}}$. To specify the reason for such temperature dependencies, we have fitted both $-\rho_{xy}^{\text{SHE}}$ and $-\rho_{xy}^{\text{AHE}}$ as a function of $\rho_{xx,T}$ with Eq. (3) as shown in Fig. 5, and obtained β_1^{H} and γ^{H} as the quadratic and linear terms in Eq. (3), respectively (see Table I). For example, β_1^{SHE} of Py is more than two orders of magnitude larger than β_1^{AHE}. Even for Py, the relations between the SHE and AHE for β_1^{H} and γ^{H} are not as simple as the skew scattering term.

A similar tendency can be seen for the other 3*d* FMs. For Fe, Co, and Ni, β_1^{SHE} is one or two orders of magnitude larger than β_1^{AHE}, as shown in Table I. Note that β_1^{AHE} values in this work are in good agreement with previous experiments (see Table I) and tight-binding calculations [58]. On the other hand, $|\beta_1^{\text{SHE}}|$ of the 3*d* FMs ranges between 4.9 and $17 \times 10^3 \ \Omega^{-1} \text{cm}^{-1}$, which is larger than that of a typical SHE material, Pt ($1.6 \times 10^3 \ \Omega^{-1} \text{cm}^{-1}$) [13,16]. The relation between γ^{SHE} and γ^{AHE} strongly varies with the 3*d* FMs (see Table I).

Much larger β_1^{SHE} values than β_1^{AHE} ones would originate from the stronger temperature dependence of the SHE in 3*d* FMs. At the moment, we do not have a conclusive picture for the origin of this dependence. In general, the spin transport can be mediated not only by conduction electrons, but also by magnons in FMs [59,60]. One possible scenario is the contribution of electron-magnon interactions in 3*d* FMs. The electron-magnon interactions would induce additional spin-flip processes. We note that such spin-flip processes are equivalent in magnitude for up-to-down and down-to-up spin channels even in ferromagnetic systems [61]. In such a situation, some asymmetric scatterings which are spin dependent would contribute only to the SHE but not to the AHE, and thus would be associated with the fact that the strong temperature dependence is not present in the AHE of the 3*d* FMs or the SHE of nonmagnetic metals. Interestingly, a recent theoretical report claims that magnon spin current can be significant around room temperature in 3*d* FMs [62], which might be related to our case. However, there are some open questions: how large the asymmetric scatterings are quantitatively and whether any other mechanisms contribute to the observed spin Hall resistivity or not. These would be addressed in the future.

IV. SUMMARY

In conclusion, we experimentally investigated the relation between the SHE and AHE in four 3*d* FMs [Fe, Co, Py (Ni$_{81}$Fe$_{19}$), and Ni]. In a typical ferromagnetic alloy, Py, the skew scattering contribution of the AHE is related to that of the SHE via the spin polarization of Py, as can be understood intuitively. However, this relation does not hold for other mechanisms. This fact is highlighted by the temperature dependence of the SHE and AHE. For all the 3*d* FMs, one of the intrinsic mechanism terms β_1^{SHE} is much larger than

TABLE I. The coefficients β_1^H and γ^H extracted from the fittings with Eq. (3) for each FM. For comparison, we also show the coefficient of the quadratic term of the AHE from previous works (Refs. [45,49,52–54]) in the table.

FM	β_1^{SHE} ($\times 10^3\ \Omega^{-1}\,cm^{-1}$)	β_1^{AHE} ($\times 10^3\ \Omega^{-1}\,cm^{-1}$)	β_1^{AHE} or b [55] in literature ($\times 10^3\ \Omega^{-1}\,cm^{-1}$)	γ^{SHE} ($\times 10^3\ \Omega^{-1}\,cm^{-1}$)	γ^{AHE} ($\times 10^3\ \Omega^{-1}\,cm^{-1}$)
Fe	4.9 ± 0.2	0.89 ± 0.04	1.1 [45], 0.82 [53]	-1.1 ± 0.1	1.50 ± 0.03
Co	-8.3 ± 0.5	0.34 ± 0.03	0.2 [54], 0.73 [49]	0.04 ± 0.24	0.97 ± 0.02
Py	-10.1 ± 0.3	-0.056 ± 0.015	-0.05 [45]	0.57 ± 0.14	-0.002 ± 0.009
Ni	-17.1 ± 0.5	-0.14 ± 0.11	$-(0.5 \sim 1.0)$ [52]	5.9 ± 0.4	-0.89 ± 0.09

β_1^{AHE}. Asymmetric spin-dependent scatterings in the spin-flip processes induced by the electron-magnon interactions would be a possible explanation for the strong temperature dependence of the SHE in contrast to the AHE or even the SHE in nonmagnetic metals.

[1] A. Hoffmann, IEEE Trans. Magn. **49**, 5172 (2013).

[2] J. Sinova, S. O. Valenzuela, J. Wunderlich, C. H. Back, and T. Jungwirth, Rev. Mod. Phys. **87**, 1213 (2015).

[3] Y. Niimi and Y. Otani, Rep. Prog. Phys. **78**, 124501 (2015).

[4] M. I. Dyakonov and V. I. Perel, Phys. Lett. A **35**, 459 (1971).

[5] J. E. Hirsch, Phys. Rev. Lett. **83**, 1834 (1999).

[6] Y. K. Kato, R. S. Myers, A. C. Gossard, and D. D. Awschalom, Science **306**, 1910 (2004).

[7] J. Wunderlich, B. Kaestner, J. Sinova, and T. Jungwirth, Phys. Rev. Lett. **94**, 047204 (2005).

[8] E. Saitoh, M. Ueda, H. Miyajima, and G. Tatara, Appl. Phys. Lett. **88**, 182509 (2006).

[9] K. Ando, S. Takahashi, K. Harii, K. Sasage, J. Ieda, S. Maekawa, and E. Saitoh, Phys. Rev. Lett. **101**, 036601 (2008).

[10] O. Mosendz, J. E. Pearson, F. Y. Fradin, G. E. W. Bauer, S. D. Bader, and A. Hoffmann, Phys. Rev. Lett. **104**, 046601 (2010).

[11] O. Mosendz, V. Vlaminck, J. E. Pearson, F. Y. Fradin, G. E. W. Bauer, S. D. Bader, and A. Hoffmann, Phys. Rev. B **82**, 214403 (2010).

[12] L. Liu, T. Moriyama, D. C. Ralph, and R. A. Buhrman, Phys. Rev. Lett. **106**, 036601 (2011).

[13] M. Morota, Y. Niimi, K. Ohnishi, D. H. Wei, T. Tanaka, H. Kontani, T. Kimura, and Y. Otani, Phys. Rev. B **83**, 174405 (2011).

[14] K. Kondou, H. Sukegawa, S. Mitani, K. Tsukagoshi, and S. Kasai, Appl. Phys. Express **5**, 073002 (2012).

[15] M. Isasa, E. Villamor, L. E. Hueso, M. Gradhand, and F. Casanova, Phys. Rev. B **91**, 024402 (2015).

[16] E. Sagasta, Y. Omori, M. Isasa, M. Gradhand, L. E. Hueso, Y. Niimi, Y. C. Otani, and F. Casanova, Phys. Rev. B **94**, 060412(R) (2016).

[17] B. Gu, I. Sugai, T. Ziman, G. Y. Guo, N. Nagaosa, T. Seki, K. Takanashi, and S. Maekawa, Phys. Rev. Lett. **105**, 216401 (2010).

[18] Y. Niimi, M. Morota, D. H. Wei, C. Deranlot, M. Basletic, A. Hamzic, A. Fert, and Y. Otani, Phys. Rev. Lett. **106**, 126601 (2011).

[19] Y. Niimi, Y. Kawanishi, D. H. Wei, C. Deranlot, H. X. Yang, M. Chshiev, T. Valet, A. Fert, and Y. Otani, Phys. Rev. Lett. **109**, 156602 (2012).

[20] P. Laczkowski, J.-C. Rojas-Sanchez, W. Savero-Torres, H. Jaffres, N. Reyren, C. Deranlot, L. Notin, C. Beigne, A. Marty, J.-P. Attane, L. Vila, J.-M. George, and A. Fert, Appl. Phys. Lett. **104**, 142403 (2014).

[21] K. Fujiwara, Y. Fukuma, J. Matsuno, H. Idzuchi, Y. Niimi, Y. Otani, and H. Takagi, Nat. Commun. **4**, 2893 (2013).

[22] K. Ando, S. Watanabe, S. Mooser, E. Saitoh, and H. Sirringhaus, Nat. Mater. **12**, 622 (2013).

[23] M. Gradhand, D. V. Fedorov, P. Zahn, and I. Mertig, Phys. Rev. Lett. **104**, 186403 (2010).

[24] S. Lowitzer, M. Gradhand, D. Ködderitzsch, D. V. Fedorov, I. Mertig, and H. Ebert, Phys. Rev. Lett. **106**, 056601 (2011).

[25] A. Fert and P. M. Levy, Phys. Rev. Lett. **106**, 157208 (2011).

[26] G. Y. Guo, S. Murakami, T.-W. Chen, and N. Nagaosa, Phys. Rev. Lett. **100**, 096401 (2008).

[27] T. Tanaka, H. Kontani, M. Naito, T. Naito, D. S. Hirashima, K. Yamada, and J. Inoue, Phys. Rev. B **77**, 165117 (2008).

[28] N. Nagaosa, J. Sinova, S. Onoda, A. H. MacDonald, and N. P. Ong, Rev. Mod. Phys. **82**, 1539 (2010).

[29] B. Zimmermann, K. Chadova, D. Ködderitzsch, S. Blügel, H. Ebert, D. V. Fedorov, N. H. Long, P. Mavropoulos, I. Mertig, Y. Mokrousov, and M. Gradhand, Phys. Rev. B **90**, 220403(R) (2014).

[30] B. F. Miao, S. Y. Huang, D. Qu, and C. L. Chien, Phys. Rev. Lett. **111**, 066602 (2013).

[31] A. Tsukahara, Y. Ando, Y. Kitamura, H. Emoto, E. Shikoh, M. P. Delmo, T. Shinjo, and M. Shiraishi, Phys. Rev. B **89**, 235317 (2014).

[32] C. Du, H. Wang, F. Yang, and P. C. Hammel, Phys. Rev. B **90**, 140407(R) (2014).

[33] K. S. Das, W. Y. Schoemaker, B. J. van Wees, and I. J. Vera-Marun, Phys. Rev. B **96**, 220408(R) (2017).

[34] K. S. Das, J. Liu, B. J. van Wees, and I. J. Vera-Marun, Nano Lett. **18**, 5633 (2018).

[35] J. D. Gibbons, D. MacNeill, R. A. Buhrman, and D. C. Ralph, Phys. Rev. Applied **9**, 064033 (2018).

[36] S. Iihama, T. Taniguchi, K. Yakushiji, A. Fukushima, Y. Shiota, S. Tsunegi, R. Hiramatsu, S. Yuasa, Y. Suzuki, and H. Kubota, Nat. Electronics **1**, 120 (2018).

[37] C. Qin, S. Chen, Y. Cai, F. Kandaz, and Y. Ji, Phys. Rev. B **96**, 134418 (2017).

[38] T. Taniguchi, J. Grollier, and M. D. Stiles, Phys. Rev. Applied **3**, 044001 (2015).

[39] M. Seemann, D. Koedderitzsch, S. Wimmer, and H. Ebert, Phys. Rev. B **92**, 155138 (2015).

[40] Within the semiclassical picture, the anomalous Hall and spin Hall conductivities arising from scatterings are given by $\sigma_{xy}^{\mathrm{AHE}} = -\frac{e^2}{\hbar} \frac{1}{(2\pi)^3} \int_{\mathrm{FS}} \frac{v_x(\mathbf{k})\lambda_y(\mathbf{k})}{|\mathbf{v}(\mathbf{k})|} dS$ and $\sigma_{xy}^{\mathrm{SHE}} = -\frac{e^2}{\hbar} \frac{1}{(2\pi)^3} \int_{\mathrm{FS}} s_z(\mathbf{k}) \frac{v_x(\mathbf{k})\lambda_y(\mathbf{k})}{|\mathbf{v}(\mathbf{k})|} dS$, respectively. Here, $v_i(\mathbf{k})$ are the Fermi velocities, $\lambda_i(\mathbf{k})$ is the mean-free path, $s_z(\mathbf{k})$ is the spin polarization, and we integrate over the Fermi surface (FS). In the limit of diffusive transport with an isotropic spin polarization $s_z(\mathbf{k}) = p$, we can take p in front of the integral and we find $\rho_{xy}^{\mathrm{AHE}} = p\rho_{xy}^{\mathrm{SHE}}$.

[41] J. Smit, Physica (Amsterdam) **24**, 39 (1958).

[42] See Supplemental Material at http://link.aps.org/supplemental/10.1103/PhysRevB.99.014403 for details of the evaluation of the spin diffusion length of the middle wire and $\bar{I}_{\mathrm{S}}$, the Onsager reciprocity in Py, and the relation between SHE and AHE using the simplified model.

[43] P. Jacquod, R. S. Whitney, J. Meair, and M. Büttiker, Phys. Rev. B **86**, 155118 (2012).

[44] S. Takahashi and S. Maekawa, Phys. Rev. B **67**, 052409 (2003); Sci. Tech. Adv. Mater. **9**, 014105 (2008).

[45] Y. Q. Zhang, N. Y. Sun, R. Shan, J. W. Zhang, S. M. Zhou, Z. Shi, and G. Y. Guo, J. Appl. Phys. **114**, 163714 (2013).

[46] D. Hou, G. Su, Y. Tian, X. Jin, S. A. Yang, and Q. Niu, Phys. Rev. Lett. **114**, 217203 (2015).

[47] Y. Tian, L. Ye, and X. Jin, Phys. Rev. Lett. **103**, 087206 (2009).

[48] S. A. Yang, H. Pan, Y. Yao, and Q. Niu, Phys. Rev. B **83**, 125122 (2011).

[49] D. Hou, Y. Li, D. Wei, D. Tian, L. Wu, and X. Jin, J. Phys.: Condens. Matter **24**, 482001 (2012).

[50] L. J. Zhu, D. Pan, and J. H. Zhao, Phys. Rev. B **89**, 220406 (2014).

[51] J. Xu, L. Wu, Y. Li, D. Tian, K. Zhu, X. Gong, and X. Jin, Sci. Bull. **60**, 1261 (2015).

[52] L. Ye, Y. Tian, X. Jin, and D. Xiao, Phys. Rev. B **85**, 220403(R) (2012).

[53] L. Wu, Y. Li, J. Xu, D. Hou, and X. Jin, Phys. Rev. B **87**, 155307 (2013).

[54] J. Kötzler and W. Gil, Phys. Rev. B **72**, 060412(R) (2005).

[55] Strictly speaking, β_0^{AHE} and β_1^{AHE} are different from b which is the coefficient of ρ_{xx}^2 in Ref. [45]. In general, b should be closer to β_1^{AHE}, but in the case of Py, both β_0^{AHE} and β_1^{AHE} are comparable to b.

[56] E. Sagasta, Y. Omori, M. Isasa, Y. Otani, L. E. Hueso, and F. Casanova, Appl. Phys. Lett. **111**, 082407 (2017).

[57] N. F. Mott, Adv. Phys. **13**, 325 (1964).

[58] T. Naito, D. S. Hirashima, and H. Kontani, Phys. Rev. B **81**, 195111 (2010).

[59] J. Cramer, F. Fuhrmann, U. Ritzmann, V. Gall, T. Niizeki, R. Ramos, Z. Qiu, D. Hou, T. Kikkawa, J. Sinova, U. Nowak, E. Saitoh, and M. Kläui, Nat. Commun. **9**, 1089 (2018).

[60] L. J. Cornelissen, J. Liu, R. A. Duine, J. Ben Youssef, and B. J. van Wees, Nat. Phys. **11**, 1022 (2015).

[61] The scattering probability related to the spin-flip process is defined as $P_{kk'}^{+-} \sim |\langle \Psi_{k'}^- | \hat{T} | \Psi_k^+ \rangle|^2$ where $\Psi_{k(k')}^{+(-)}$ is the wave function before (after) the scattering with the wave number k (k') and spin-up $+$ (spin-down $-$), and $\hat{T}$ is a matrix in spin space including spin-orbit coupling and magnetism. By defining $P_{kk'}^{-+}$ in an equivalent way and integrating k and k', we find that on average it holds $\tau_{+-}^{-1} = \tau_{-+}^{-1}$, with $\tau^{-1} = \int dk \int dk' P_{kk'}$, even in the magnetic case.

[62] Y. Cheng, K. Chen, and S. Zhang, Phys. Rev. B **96**, 024449 (2017).